Journal of Power Sources 266 (2014) 332–340

Contents lists available at ScienceDirect

Journal of Power Sources

journal homepage: www.elsevier.com/locate/jpowsour

Effects of anode flooding on the performance degradation of polymer electrolyte membrane fuel cells

Mansu Kim [a,1], Namgee Jung [a,1], KwangSup Eom [b], Sung Jong Yoo [a], Jin Young Kim [a], Jong Hyun Jang [a], Hyoung-Juhn Kim [a], Bo Ki Hong [c], EunAe Cho [a,*]

[a] Fuel Cell Research Center, Korea Institute of Science and Technology (KIST), Seoul 136-791, Republic of Korea
[b] School of Chemical & Biomolecular Engineering, Center for Innovative Fuel Cell and Battery Technologies, Georgia Institute of Technology, Atlanta, GA 30332, USA
[c] Fuel Cell Vehicle Team 1, Eco-Technology Center, Hyundai-Kia Motors, 104, Mabuk-Dong, Giheung-Gu, Yongin-Si, Gyeonggi-Do 446-912, Republic of Korea

HIGHLIGHTS

- Anode flooding can occur by direct flow of condensed water in humidified fuel.
- Anode flooding induces local fuel starvation and high potential in the anode.
- High potential locally present in the anode results in anode carbon corrosion.
- Anode carbon corrosion plays a key role in MEA degradation by anode flooding.

ARTICLE INFO

Article history:
Received 14 February 2014
Received in revised form
16 April 2014
Accepted 20 April 2014
Available online 10 May 2014

Keywords:
Anode flooding
Fuel starvation
Carbon corrosion
Water management
Polymer electrolyte membrane fuel cell (PEMFC)

ABSTRACT

Polymer electrolyte membrane fuel cell (PEMFC) stacks in a fuel cell vehicle can be inevitably exposed to harsh environments such as cold weather in winter, causing water flooding by the direct flow of condensed water to the electrodes. In this study, anode flooding was experimentally investigated with condensed water generated by cooling the anode gas line during a long-term operation (~1600 h). The results showed that the performance of the PEMFC was considerably degraded. After the long-term experiment, the thickness of the anode decreased, and the ratio of Pt to carbon in the anode increased. Moreover, repeated fuel starvation of the half-cell severely oxidized the carbon surface due to the high induced potential (>1.5 V_{RHE}). The cyclic voltammogram of the anode in the half-cell experiments indicated that the characteristic feature of the oxidized carbon surface was similar to that of the anode in the single cell under anode flooding conditions during the long-term experiment. Therefore, repeated fuel starvation by anode flooding caused severe carbon corrosion in the anode because the electrode potential locally increased to >1.0 V_{RHE}. Consequently, the density of the tri-phase boundary decreased due to the corrosion of carbons supporting the Pt nanoparticles in the anode.

1. Introduction

Polymer electrolyte membrane fuel cells (PEMFC) have been extensively developed as an electrochemical energy conversion device and the main power source for hydrogen vehicles because of their high efficiency and environment-friendly operation [1]. PEMFCs consist of many components developed by various technologies related to electrochemistry, materials science, and chemical and mechanical engineering; membrane electrode assemblies (MEAs), gas diffusion layers (GDLs), and bipolar plates with gas flow channels. Global automakers have achieved significant accomplishments to commercialize fuel cell vehicles (FCVs) over the past decade. Recently, Hyundai motor company started the commercial production of the Tucson ix35 FCV with a well-designed fuel cell stack, which can cover ~594 km under new European driving cycle conditions without hydrogen refueling. However, to be more commercially viable, the fuel cell stacks should be improved further by overcoming technical issues such as high Pt loadings [2,3], difficulty in water management [4,5], corrosion of bipolar plates [6,7], and low hydrogen storage capacity of the fuel tank [8,9].

* Corresponding author. Tel.: +82 2 958 5279; fax: +82 2 958 5199.
E-mail address: eacho@kist.re.kr (E. Cho).
[1] These authors contributed equally.

http://dx.doi.org/10.1016/j.jpowsour.2014.04.092
0378-7753/

Among these obstacles, water management in the MEAs is one of the most crucial issues affecting the performance of the fuel cell stack [10]. The cathode of a PEMFC electrochemically produces water by the oxygen reduction reaction (ORR), and some of the water thus generated can be transferred to the anode by the back-diffusion mechanism [11]. In contrast, the protons generated at the anode are transferred with water to the cathode by electroosmotic drag [12]. Furthermore, under normal fuel cell operation, H_2 and air with high relative humidity (RH) are supplied to the anode and cathode of fuel cell stacks, respectively [2,4,13]. Therefore, if the water present in the catalyst layers is not properly managed, it severely inhibits the transport of H_2 and O_2 to the catalyst surface through the electrodes with a thickness of several micrometers.

The effects of cathode flooding on fuel cell performance have been already studied [10,14,15]. It has been reported that liquid water blocks the catalytic active sites in the cathode, resulting in extremely low performance of the fuel cell because of the high mass-transfer resistances in the high current density region and the high overpotential of the ORR itself. To remove water from the cathode efficiently, hydrophobic additives, such as polytetrafluoroethylene (PTFE), have been added to the cathode catalyst layers [14,15], or the surface of carbon support materials has been selectively functionalized with a temperature-directed switchable polymer to thermally change the hydrophilicity of the catalyst layers [10].

Despite the technical importance, anode flooding has been rarely investigated since the anodic reaction, hydrogen oxidation reaction (HOR), has a low overpotential compared to the ORR. Under practical operating conditions such as cold weather during winter, anode flooding in the MEAs can be accelerated due to the direct flow of condensed water to the anode; humidified hydrogen can be cooled down during passing through the gas lines connecting the humidifier to the stack. Moreover, during long-term operation, excess water can be transferred from the cathode to the anode by back diffusion. Continuous water accumulation in the anode may cause severe anode flooding and localized fuel starvation in the fuel cell stacks. This may become an important factor for anode degradation, and severe problems such as carbon corrosion can be electrochemically observed in the anode.

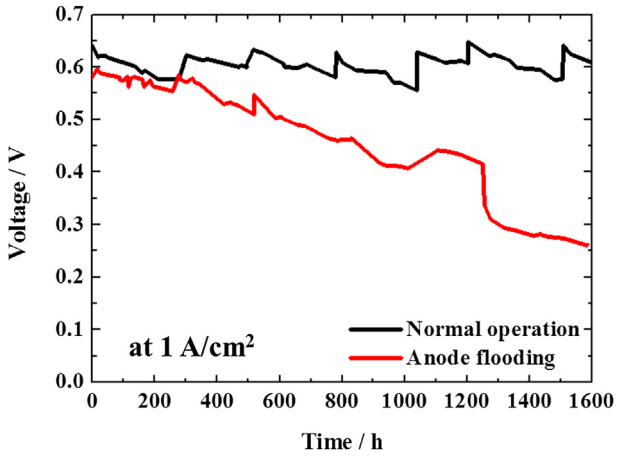

Fig. 2. The voltage decay profiles of the single cells for 1600 h at the constant current density of 1 A cm^{-2}.

As shown in previous studies on fuel starvation at the anode, the oxidation reaction of carbon supports (carbon corrosion) predominated over the HOR at the anode due to the abnormally increased electrode potential of >1.0 V_{RHE} when H_2 gas was not sufficiently supplied to the anode [16–19]. The carbon corrosion mechanism can be expressed as follows:

$$C + 2H_2O \rightarrow CO_2 + 4H^+ + 4e^- (0.207\ V_{RHE})$$

$$C + H_2O \rightarrow CO + 2H^+ + 2e^- (0.518\ V_{RHE})$$

where RHE is the reversible hydrogen electrode.

Although carbon corrosion reactions in the anode are generally not thermodynamically or kinetically favored under normal operating conditions, those reactions can be accelerated when the electrode potential increases to >1.0 V_{RHE} due to hydrogen fuel starvation [20–26]. Therefore, anode flooding is very similar to fuel starvation, in that severe concentration overpotential is induced

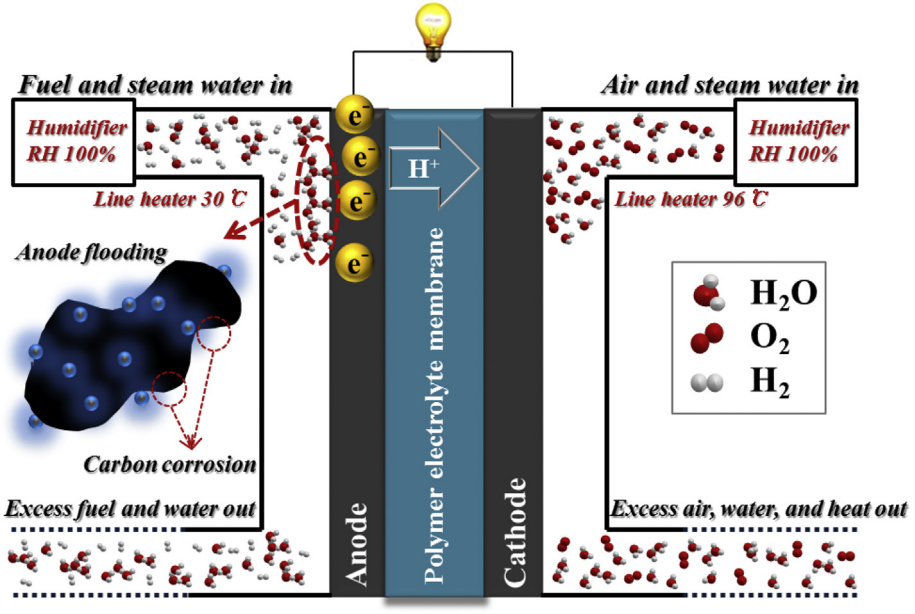

Fig. 1. A schematic diagram of the experimental set-up to simulate the anode flooding status during long-term performance test of single cell.

locally by the decreasing hydrogen diffusion rate owing to the presence of condensed liquid water in the anode catalyst layer. Therefore, anode flooding may significantly affect the durability and catalytic activity of catalysts due to severe carbon corrosion.

Darling and Gasteiger research groups reported cathode carbon corrosion caused by localized fuel starvation [25,27]. A vacant space, in which the access to H_2 gas was limited, was formed in the anode catalyst layer as a result of blocked fuel flow in the active area during fuel cell operation. Then, since the diffusion of O_2 from the cathode to the vacant space in the anode through the membrane increased, carbon corrosion occurred in the cathode due to the formation of a H_2/air boundary in the anode [28,29]. On the other hand, Wilkinson and Hou research groups introduced N_2 gas instead of H_2 gas as the fuel or a mixture of H_2 and N_2 gases to the anode to simulate fuel starvation at the anode, resulting in irreversible damage to the fuel cell stack [16,17,30]. In these cases, it was difficult to form a H_2/air boundary in the anode catalyst layer because the anode was already filled with inert N_2 gas. Consequently, the anode potential immediately increased on fuel starvation, and carbon corrosion occurred in the anode catalyst layer, but not in the cathode. When H_2 gas was abruptly replaced by N_2 gas, the cell potential dramatically decreased to -1.0 V_{RHE} within 10 min due to extreme fuel starvation.

Herein, we investigated degradation of MEA caused by anode flooding that might occur frequently during winter. The temperature of the anode line heater was intentionally maintained at 30 °C to simulate anode flooding condition resulting from the presence of condensed water in the exterior H_2 gas line (Fig. 1). To closely examine the cause of fuel cell performance degradation, the electrodes were analyzed by scanning electron microscopy (SEM), transmission electron microscopy (TEM), energy-dispersive X-ray spectroscopy (EDS), electron probe microanalyzer (EPMA), and electrochemical measurements such as electrochemical impedance spectroscopy (EIS) and cyclic voltammetry (CV). The results of half-cell experiments confirmed that repeated anode flooding conditions drastically degraded the fuel cell catalysts.

2. Experimental

2.1. Single cell preparation and activation process

The commercial perfluorinated sulfonic acid (PFSA) MEAs (Gore Co.) with an active area of 25 cm^2 and graphite bipolar plates (ILDO F&C Co., Ltd.) with four-serpentine channels for both anode and cathode flow fields, which had mirror-image symmetry and co-flow orientation. The channel and land widths were 1.0 and 0.75 mm, respectively. The channel depths of the anode and cathode sides were 0.40 and 0.60 mm, respectively. Both the anode and cathode were composed of conventional Pt/C catalyst with Pt loadings of 0.1 and 0.4 mg cm^{-2}, respectively. A commercial GDL with a thickness of 415 μm was used. The GDL was composed of a microporous layer and macroporous carbon fiber felts that were wet-proofed by hydrophobic treatment. The assembled single cell was fully activated by maintaining a constant voltage of 0.45 V for 24 h at 80 °C using H_2 and air with an RH of ~100%. The stoichiometric ratios (SRs) of H_2 and air were 1.5 and 2.0, respectively. Two fully activated single cells were identically prepared to compare their behaviors under different anode operating conditions.

2.2. Long-term performance experiments using constant current density

During the long-term performance experiment, the cell temperatures were maintained at 80 °C, and the RHs were maintained at 100% for both the anode and cathode humidifiers. Although the anode line heater of the single cell was controlled at 96 °C as the normal operating condition, that of the other single cell was maintained at 30 °C to simulate the anode flooding conditions by condensing humidified H_2 gas in the gas line. The SRs of H_2 and air were 1.5 and 2.0, respectively, at a given current density of

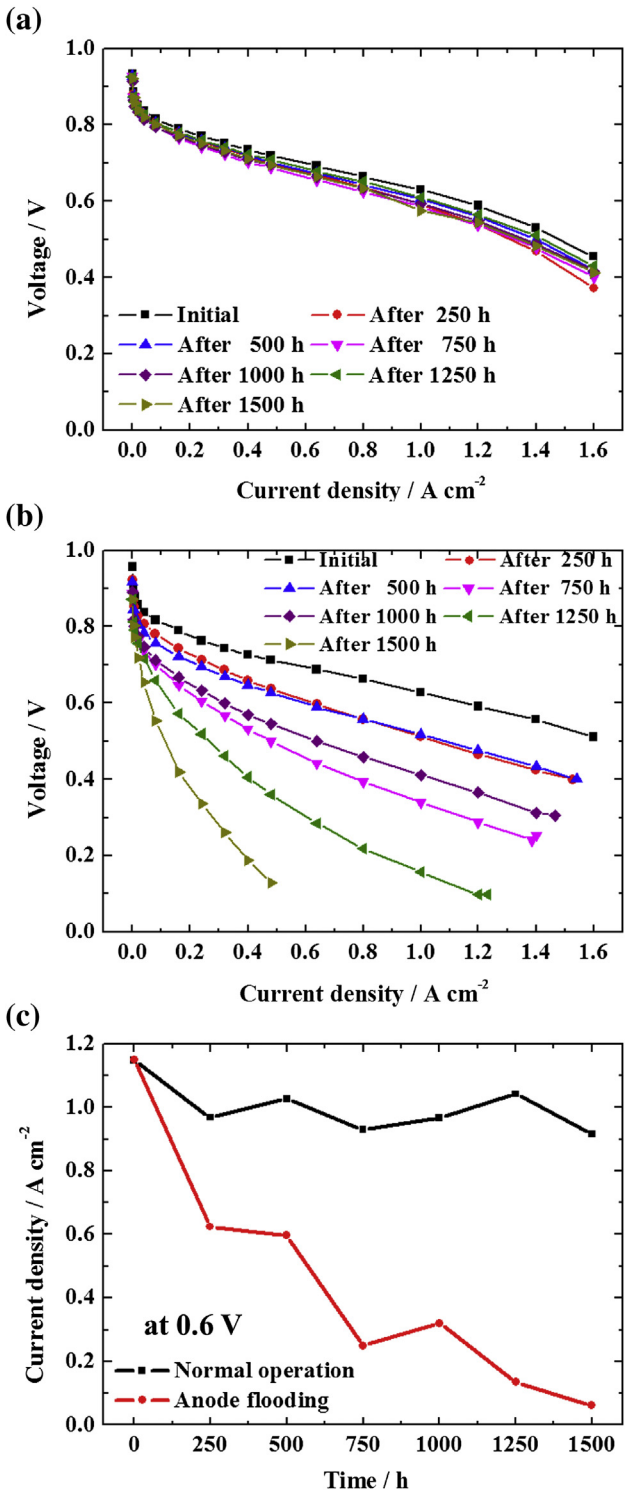

Fig. 3. The effects of the anode flooding on the single cell performance at every 250 h during the long-term performance test. The polarization curves of the single cells under (a) normal and (b) anode flooding conditions. (c) represents the change of the current densities at 0.6 V as a function of test times.

1 A cm^{-2}. Two single cells under different anode line heating conditions were investigated for up to ~1500 h.

2.3. Electrochemical characterizations of the single cells during long-term experiment

The electrochemical properties of the single cells were characterized by the polarization curve (current–voltage or *i–V*), CV, and EIS at every 250 h during the long-term experiment. In the measurements of the polarization curves, the RHs, SRs, and temperatures were the same as in the long-term experiment. The EIS was measured from 50 mHz to 10 kHz. The amplitude of the sinusoidal current signal was 5 mV at an applied potential of 0.85 V. The EIS measurements were conducted under two gas supply conditions: normal and reverse. Under the normal gas condition, H_2 and air were supplied to the anode and cathode,

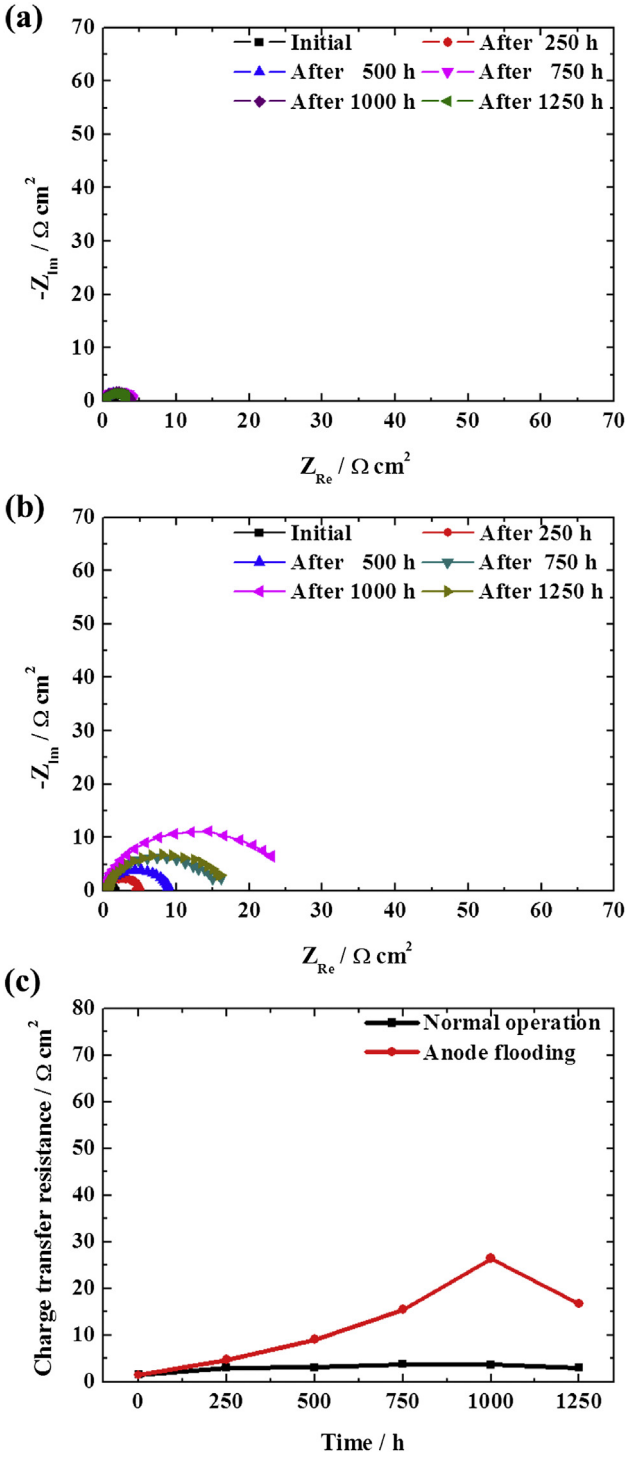

Fig. 4. The Nyquist plots to characterize the electrochemical resistances of the single cells under (a) the normal and (b) the anode flooding conditions during the long-term test. (c) represents changes of R_{ct} of the cathodes in the single cells as a function of test time. Hydrogen and air gases were flowed into the anode and cathode, respectively.

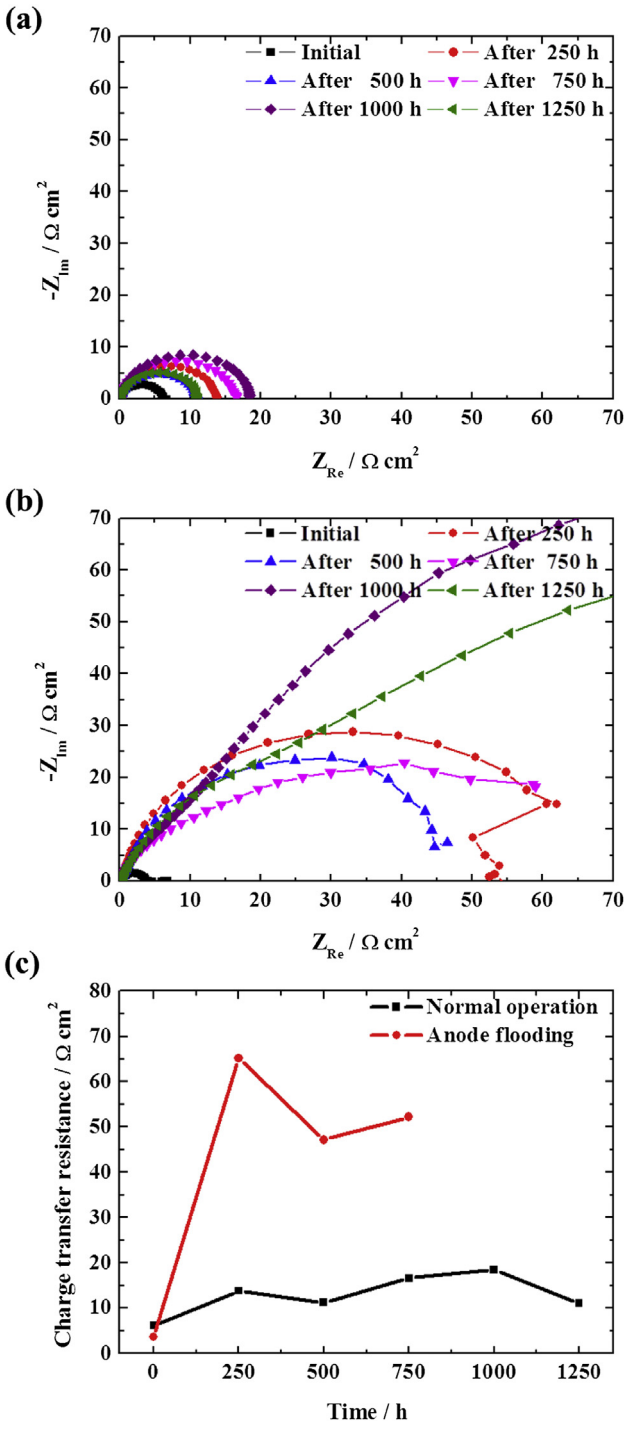

Fig. 5. The Nyquist plots to characterize the electrochemical resistances of the single cells under (a) the normal and (b) the anode flooding conditions during the long-term test. (c) represents changes of R_{ct} of the anodes in the single cells as a function of test time. Air and hydrogen gases were flowed into the anode and cathode, respectively.

respectively. In contrast, under the reverse condition, H_2 and air were supplied to the cathode and anode, respectively, to clearly elucidate the anode degradation caused by anode flooding. For the cathode, the CVs were measured from 50 mV to 1.2 V at a scan rate of 50 mV s^{-1} when humidified H_2 and N_2 were supplied to the anode and cathode, respectively. For the anode, the CVs were measured by reversing the gases to the anode (N_2) and cathode (H_2) to investigate the anode parts in more detail. The electrochemically active surfaces (EASs) of the electrodes were estimated from the coulombic charge for hydrogen desorption (Q_H).

2.4. Post-mortem analyses of the MEAs

The electrode thickness of the MEAs was measured by SEM (XL30 ESEM, FEI). The compositions of Pt and carbon in the electrodes were analyzed by the EDS in the SEM. The cross-sectional

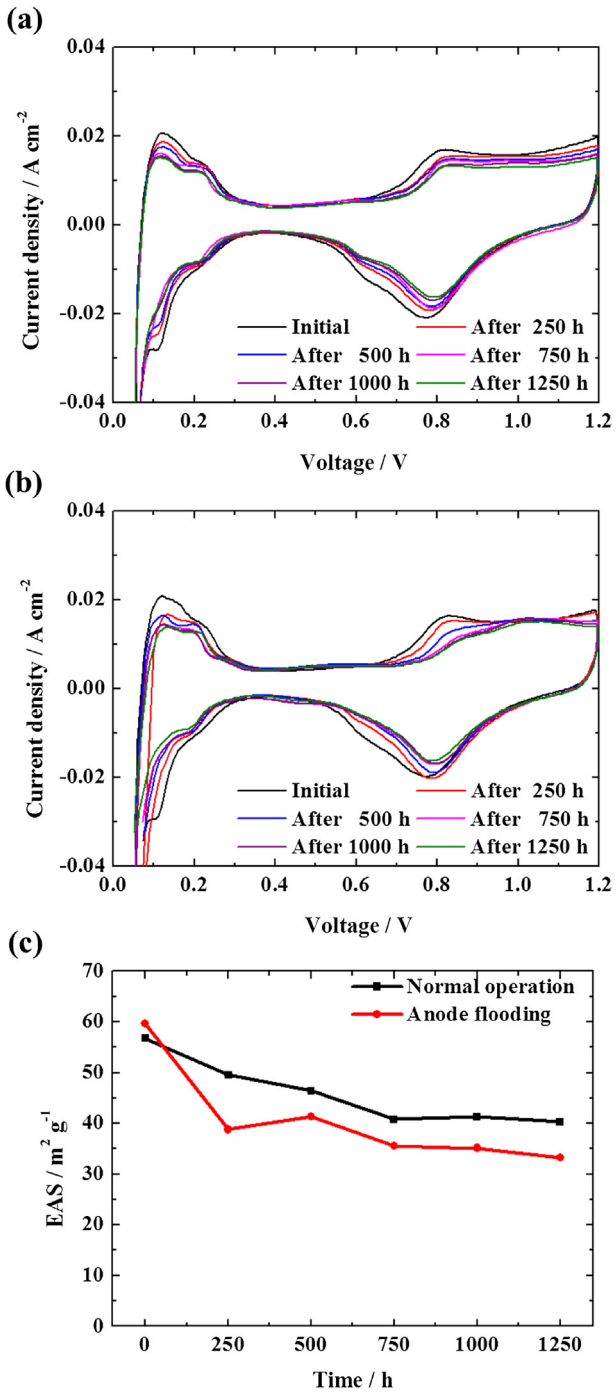

Fig. 6. The CVs to characterize the electrochemical properties of the single cells under (a) the normal and (b) the anode flooding conditions during the long-term test. (c) represents changes of EAS of the cathodes in the single cells as a function of test time. Hydrogen and nitrogen gases were flowed into the anode and cathode, respectively.

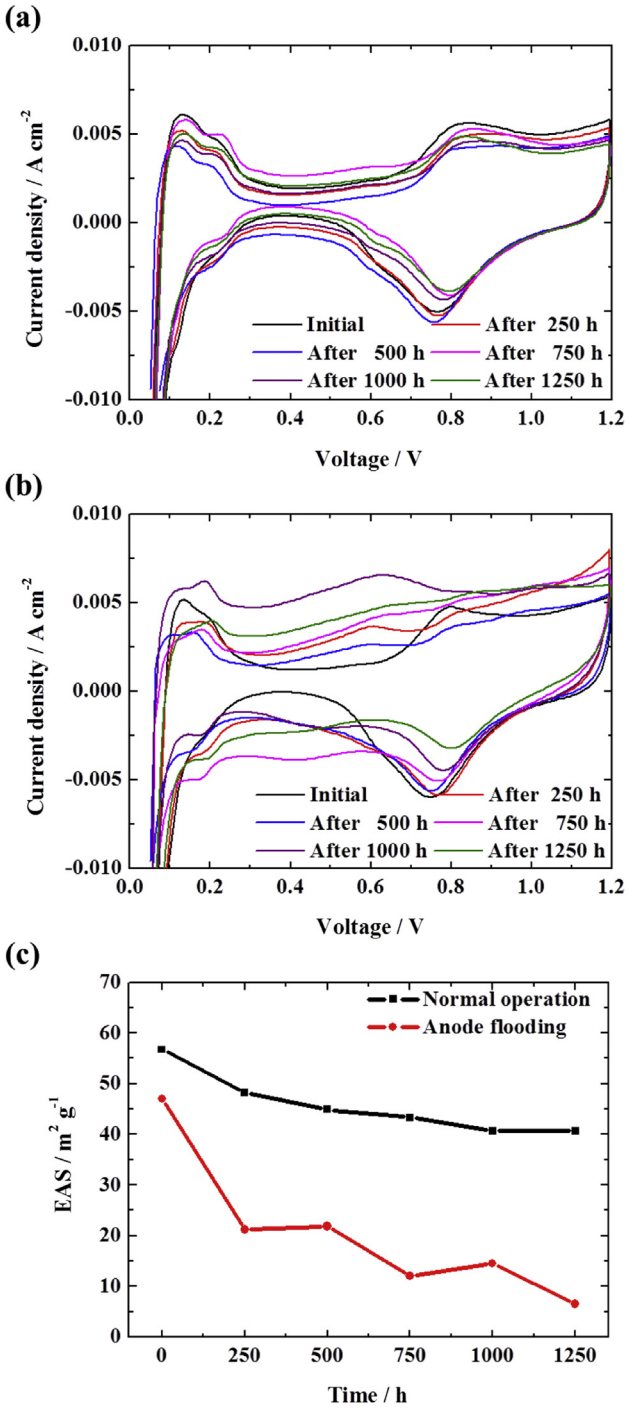

Fig. 7. The CVs to characterize the electrochemical properties of the single cells under (a) the normal and (b) the anode flooding condition during the long-term test. (c) represents changes of EAS of the anodes in the single cells as a function of test time. Nitrogen and hydrogen gases were flowed into the anode and cathode, respectively. This is a reverse gas flow condition in Fig. 6.

Pt distributions in the MEAs were observed by the EPMA (JXA-8500F, Jeol). The particle size and distribution of Pt catalysts were analyzed by TEM (CM30, Philips) before and after the long-term experiment.

2.5. Accelerated degradation test (ADT) for repeated fuel starvation in half-cell

The electrochemical measurements were analyzed using an Autolab PGSTAT20 potentiostat (Metrohm Autolab B.V.). The analyses were conducted in a three-electrode electrochemical cell using a rotating disk electrode (RDE) system (Eco Chemie B.V.) at room temperature. Pt wire and saturated calomel electrode (SCE) were used as the counter and reference electrodes, respectively. The working electrode was a catalyst-coated glassy carbon (GC) electrode with an area of 0.196 cm^2. All the potentials were measured using the RHE. The catalyst ink slurry was prepared by mixing commercial 40 wt% Pt/C (Johnson Matthey), 5 wt% Nafion solution (Aldrich), and 2-propanol. The electrolyte (0.1 M $HClO_4$) was prepared with deionized water and 70% $HClO_4$ (Aldrich). To simulate repeated fuel starvation, the chronopotentiometry was conducted at 0.2 mA by switching the gas flow from H_2 (200 s) to Ar (700 s) for 900 s (900 s = one cycle). The chronopotentiometry was repeated for 20 cycles, and the CVs were recorded with the potential cycling (0.05–1.0 V_{RHE}) to measure the amount of oxidized carbon in the catalyst at every five cycles of the fuel starvation. The Pt particle size was analyzed by TEM before and after the ADT in the half-cell.

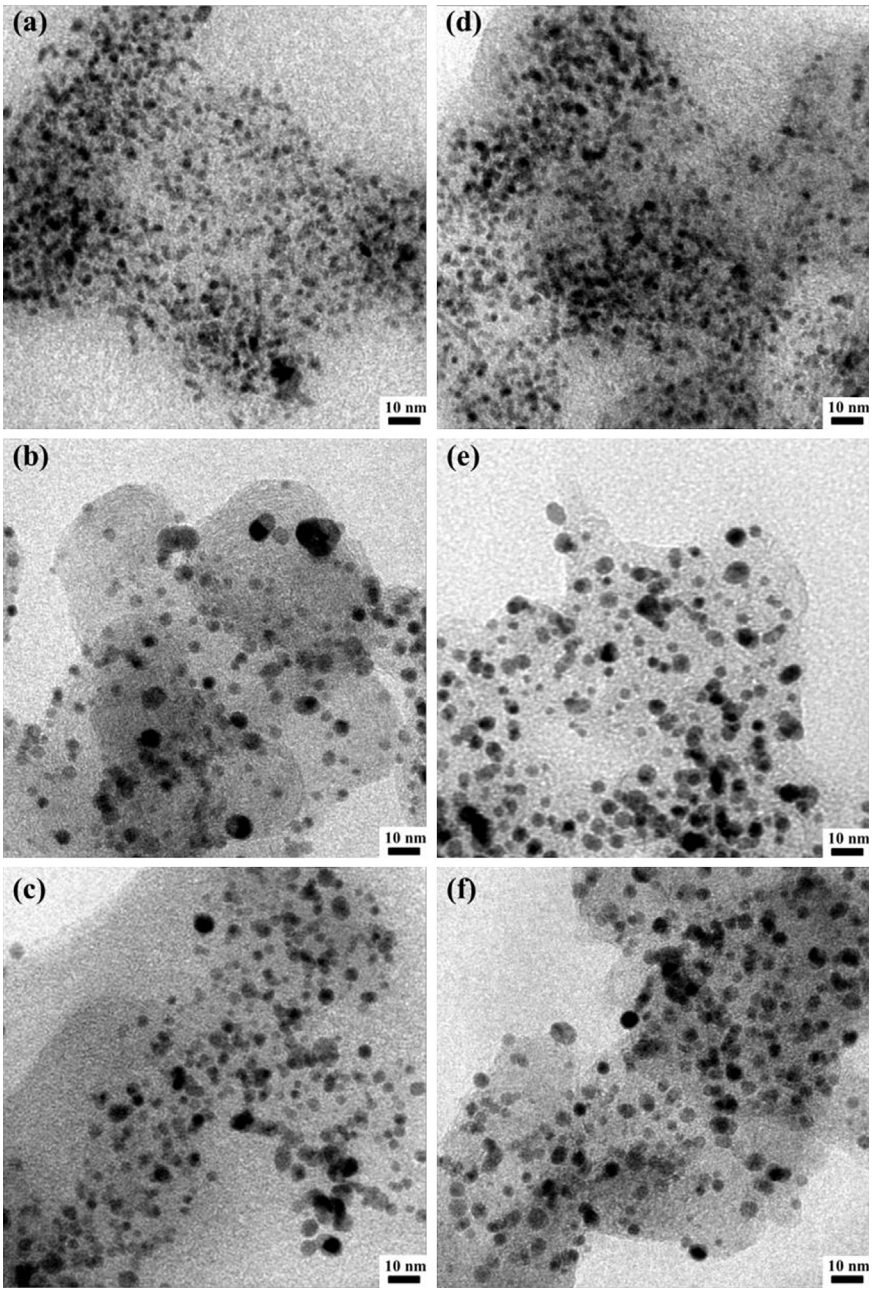

Fig. 8. TEM images for the anode (left: a–c) and cathode (right: d–f) catalysts. Fresh Pt/C catalyst before the long-term performance test (a, d), and degraded Pt/C catalysts after the long-term test under the normal (b, e) and the anode flooding (c, f) conditions.

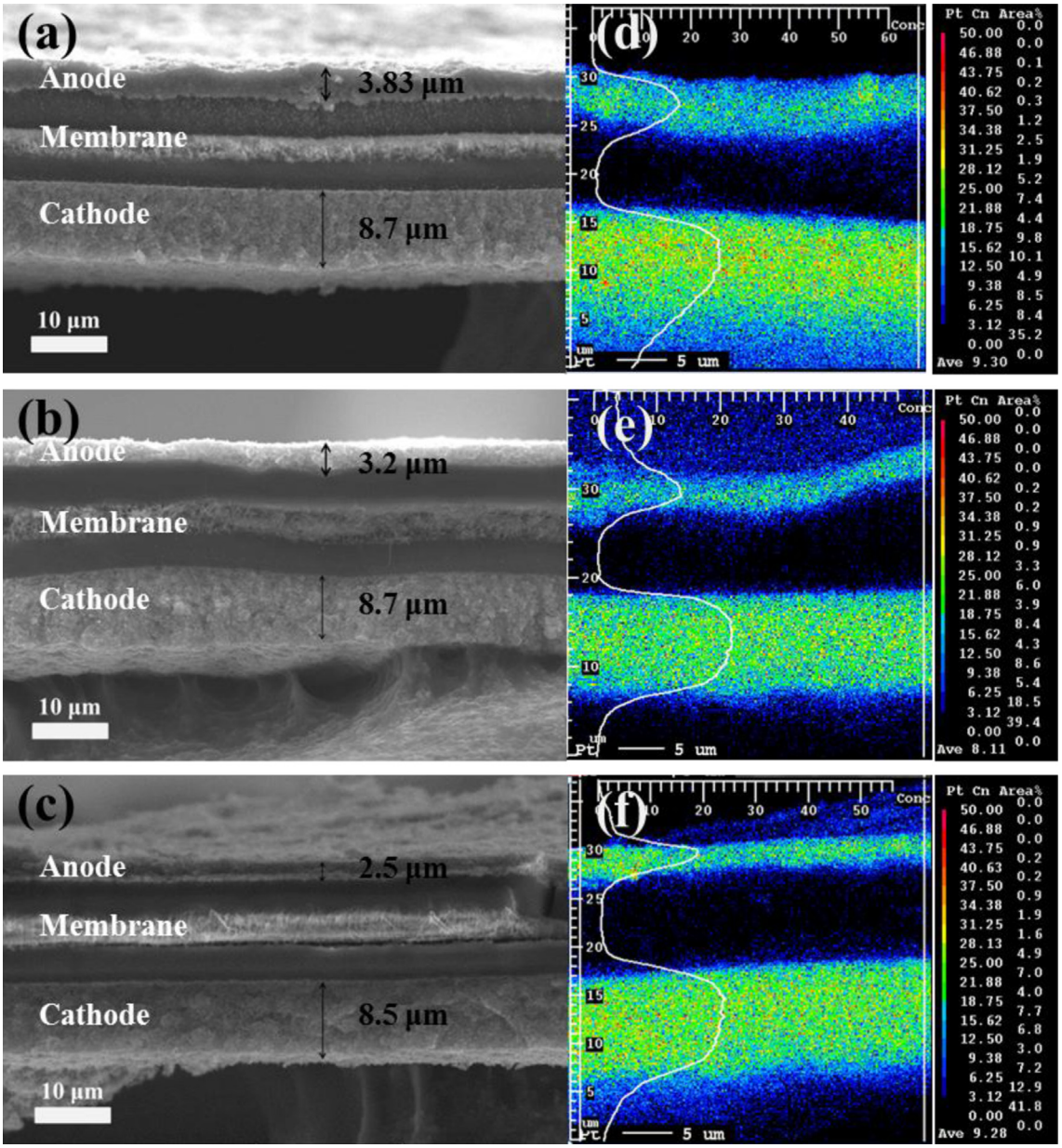

Fig. 9. Cross-sectional SEM (left: a–c) and EPMA mapping for Pt (right: d–f) images for the MEAs. Fresh MEA before the long-term performance test (a, d), and degraded MEAs after the long-term test under the normal (b, e) and the anode flooding (c, f) conditions.

3. Results and discussion

3.1. Effects of anode flooding on single-cell performance

Fig. 2 shows the voltage decay profiles of the single cells for 1600 h at a constant current density of 1 A cm^{-2}. Although the single cell voltage under the normal conditions decreased at an average voltage decay rate of 21 μV h^{-1}, under the anode flooding conditions, the average voltage decay rate considerably increased to 200 μV h^{-1}. The intermittent increases in the voltage profiles in the middle of the long-term operation can be attributed to the electrochemical measurements, such as *i–V* curve, CV, and EIS, of the two single cells [31]. The effects of the anode flooding on the single-cell performance were investigated at every 250 h during the long-term experiment (Fig. 3). The single-cell performance under the normal conditions hardly changed from 0 to 1600 h, whereas that under the anode flooding conditions rapidly decreased during the long-term experiment. Furthermore, the current density at a voltage of 0.6 V for the single cell under the anode flooding conditions dramatically decreased than under the

Table 1
The Pt and carbon compositions in the electrodes before and after long-term test measured from the EDS using the SEM.

	Fresh MEA		Degraded MEA			
			Normal condition		Anode flooding condition	
	Anode	Cathode	Anode	Cathode	Anode	Cathode
Pt (wt%)	44.8	53.8	46.5	52.4	63.7	50.3
C (wt%)	55.2	46.2	53.5	47.6	36.3	49.7
Ratio of Pt to C	0.81	1.16	0.87	1.10	1.75	1.01

normal conditions for 1600 h (Fig. 3c). Therefore, the anode flooding conditions definitely affected the fuel cell performance and durability.

3.2. Electrochemical analyses for single cells during long-term experiment

The drastic performance degradations by the anode flooding were evaluated by EIS measurements (Figs. 4 and 5) under two different gas supply conditions, normal and reverse, as described in the experimental section. In the Nyquist plots for the single cells, the intersection of the *X*-axis at a high frequency corresponds to the ohmic resistance (R_{ohm}), and the diameter of the semicircle indicates the charge-transfer resistance (R_{ct}). The R_{ohm} of the single cells hardly changed irrespective of the anode line heater temperature and long-term experiment duration (Figs. 4 and 5). Therefore, the anode flooding did not significantly affect the ionic and electronic conductivity in the MEAs. However, the R_{ct} of the single cell under the anode flooding conditions increased significantly with the experiment time (Fig. 4c). Moreover, the R_{ct} of the single cell under the anode flooding conditions increased remarkably when air was supplied to the anode (Fig. 5c). When the gas flows were reversed, the larger increase in the R_{ct} of the 'previous' anode sides (currently acting as the cathode because the gas flows were reversed) can be attributed to the larger overpotential for the ORR by the degradation of anode catalysts. Thus, the anode suffered more severe degradation than the cathode under the anode flooding conditions. The EIS results are consistent with the changes in the performance, indicating that the decrease in performance under the anode flooding conditions was caused by the degradation of anode catalysts.

In addition, the CVs were measured to clearly elucidate the EIS results (Figs. 6 and 7). The EAS was calculated from the charge integration of the hydrogen desorption peak [32,33], and the changes in the EAS are shown as a function of the experiment time (Figs. 6 and 7c). During the long-term experiment (Fig. 6c), the decrease in the EAS of the cathode (−44.3%) under the anode flooding conditions was larger than that (−29.1%) under the normal conditions. However, the decrease in the EAS of the anode (−86.2%) under the anode flooding conditions was much larger than that (−28.2%) under the normal conditions (Fig. 7c). These results show that the anode flooding destroyed the structure of anode catalysts more severely than that of the cathode catalysts, consistent to the EIS data. Therefore, the results show that mainly the degradation of the anode catalyst structure caused the voltage decay under the anode flooding conditions similar to the EIS results. Moreover, the CVs show that the density of the tri-phase boundary (TPB) in the anode may have significantly decreased under the anode flooding conditions.

3.3. Post-mortem analyses of MEAs

To directly investigate the physical and chemical degradations of the MEAs after the long-term experiment, the MEAs were analyzed by TEM, SEM, EPMA, and EDS. To evaluate the effects of the anode flooding on the growth of Pt nanoparticles, the TEM images of the catalysts in the two MEAs were recorded (Fig. 8). In the anodes, the Pt particle sizes increased from 2.95 nm (fresh sample) to 4.14 and 4.21 nm for the degraded samples under the normal and anode flooding conditions, respectively. In the cathodes, the Pt particle sizes also increased from 2.95 nm (fresh sample) to 4.25 and 4.34 nm for the degraded samples under the normal and anode flooding conditions, respectively. Thus, these results indicate that the anode flooding did not significantly affect the Pt particle size, and the increases in the Pt particle size insignificantly affect the degradation of the single-cell performance.

However, the anode thicknesses of two MEAs decreased (electrode thinning) after the long-term experiment (Fig. 9a–c). In particular, the anode thickness of the MEA under the anode flooding conditions decreased more (by 34.7%) than that under the normal conditions (by 16.4%). These results show that anode flooding can accelerate catalyst degradation. Moreover, the EPMA

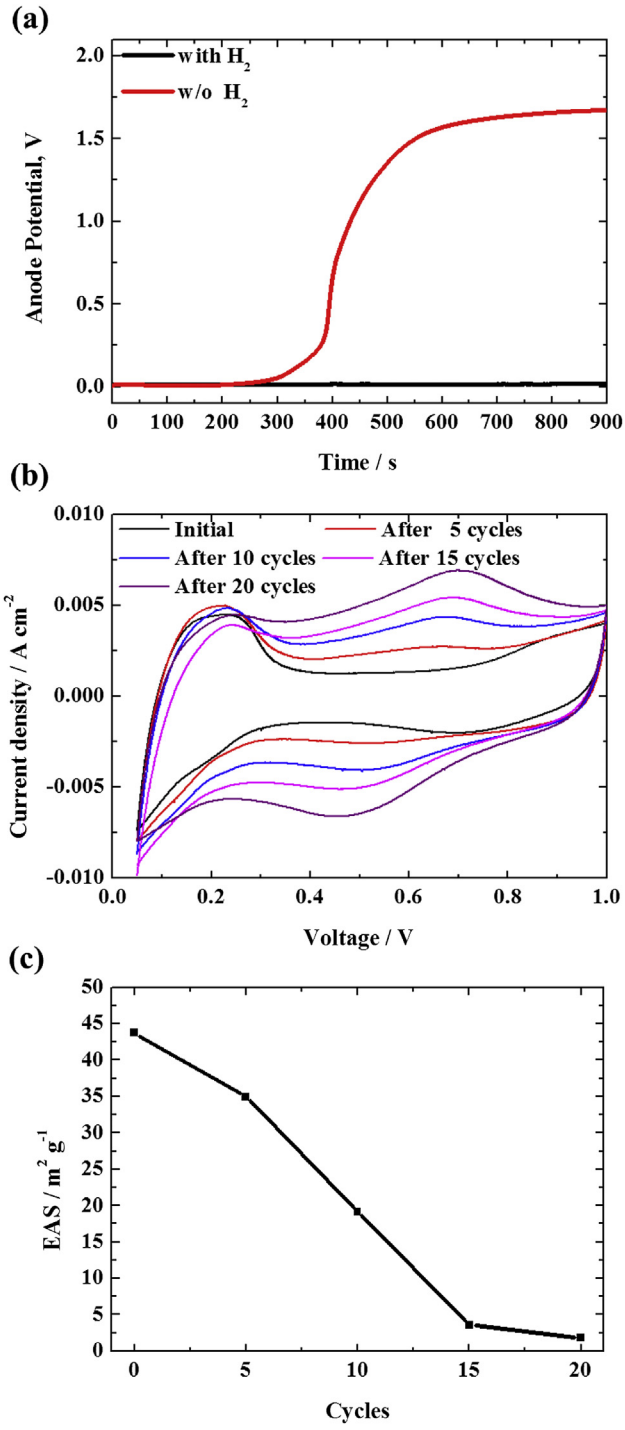

Fig. 10. (a) The chronopotentiometry at 0.2 mA with switching the gas flow from hydrogen (200 s) to argon (700 s) for 900 s in a half cell (1 cycle); (b) The CVs between 0.05 and 1.0 V_{RHE} to measure the electrochemical properties of the catalyst at every 5 cycles of the fuel starvation; (c) Changes of the EAS of the catalyst during 20 cycles.

mapping images for the cross-sectional MEAs showed that the Pt concentration in the anode under the anode flooding conditions increased more sharply than that under the normal conditions (Fig. 9d–f). Moreover, the EDS measurements using SEM showed that the ratio of Pt to carbon in the anode under the anode flooding conditions significantly increased from 0.81 (for the fresh MEA) to 1.75 (after the anode flooding), while that under the normal conditions (0.87) hardly changed compared to the fresh MEA anode (Table 1). Therefore, the increase in the Pt concentration of the anode can be attributed to the carbon corrosion in the MEA under the anode flooding conditions. Consequently, the loss of carbon supports for Pt nanoparticles with PFSA Nafion ionomers resulted in the deformation of TPB composed of H_2 gas, Pt, and Nafion ionomer as shown in the CV data.

3.4. *Effects of repeated fuel starvation by anode flooding on the catalysts in half-cell*

To study the effects of repeated fuel starvation caused by the anode flooding on the catalysts in the half-cell using the ADT, chronopotentiometry was conducted at a constant current of 0.2 mA with 40 wt% Pt/C catalysts loaded on a GC electrode. After purging H_2 gas for 200 s, the gas flow was switched from H_2 to Ar (Fig. 10a). In the presence of H_2 gas, the potential showed a constant value of <0.1 V_{RHE} due to the HOR. However, the potential increased to >1.5 V_{RHE} when the gas was switched from H_2 to Ar. It is well known that such a high potential causes severe carbon corrosion in catalysts [34]. At every five cycles, the CV was measured to detect the structural change in the catalyst surface during the ADT. As shown in Fig. 10b, the redox peaks between 0.4 and 0.7 V_{RHE} in the CVs after five cycles provided an important evidence for the oxidized carbon surface, well known as the hydroquinone–quinone (HQ–Q) redox couple of oxidized carbon [35]. A severe decrease in the EAS also confirms the catalyst structure degradation in the half-cell experiment (Fig. 10c). These results are similar to those of the CV data of the anode in the single cell under the anode flooding conditions (Fig. 7b). Therefore, based on both the single cell and half-cell data, it was confirmed that the carbons in the anodes rapidly degraded due to repeated fuel starvation under the anode flooding conditions.

4. Conclusions

The effects of anode flooding on the performance degradation of a PEMFC during a long-term operation were investigated. The long-term stability of the single cell significantly decreased under anode flooding conditions by reducing the TPB in the anode catalyst layers. The TEM images showed that the anode flooding did not significantly affect the growth of Pt nanoparticles. However, from the SEM, EPMA, EDS, CV, and EIS data, it was concluded that the performance degradation can be mainly attributed to the loss of carbon supports in the anode. Moreover, anode flooding may have caused local fuel starvation in the anode, and the half-cell experiment under a repeated fuel starvation environment showed that the carbon was actually oxidized due to the locally induced high electrode potential.

Acknowledgments

This work was supported by the New & Renewable Energy Technology Development Program of the Korea Institute of Energy Technology Evaluation and Planning (KETEP) grant funded by the Korea government Ministry of Knowledge Economy (No. 20113010030050).

References

[1] G.D. Marin, G.F. Naterer, K. Gabriel, Int. J. Hydrogen Energy 35 (2010) 6097–6107.
[2] Y.-H. Cho, H.-S. Park, Y.-H. Cho, D.-S. Jung, H.-Y. Park, Y.-E. Sung, J. Power Sources 172 (2007) 89–93.
[3] Y.-H. Cho, J.W. Lim, Y.S. Kang, Y.-H. Cho, O.-H. Kim, N.-H. Kwon, O.-J. Kwon, W.-S. Yoon, H. Choe, Y.-E. Sung, Int. J. Hydrogen Energy 37 (2012) 2490–2497.
[4] M. Ahn, Y.-H. Cho, Y.-H. Cho, J. Kim, N. Jung, Y.-E. Sung, Electrochim. Acta 56 (2011) 2450–2457.
[5] N. Yousfi-Steiner, Ph Moçotéguy, D. Candusso, D. Hissel, A. Hernandez, A. Aslanides, J. Power Sources 183 (2008) 260–274.
[6] H. Wang, M.-A. Sweikart, J.A. Turner, J. Power Sources 115 (2003) 243–251.
[7] R.-A. Antunes, M.C.L. Oliveira, G. Ett, V. Ett, Int. J. Hydrogen Energy 35 (2010) 3632–3647.
[8] C. Pohlmann, L. Rontzsch, F. Heubner, T. WeiBgarber, B. Kieback, J. Power Sources 231 (2013) 97–105.
[9] F. Fang, Y. Li, Q. Zhang, L. Sun, Z. Shao, D. Sun, J. Power Sources 195 (2010) 8215–8221.
[10] N. Jung, S.-M. Kim, D.-H. Kang, D.-Y. Chung, Y.-S. Kang, Y.-H. Chung, Y.-W. Choi, C. Pang, K.-Y. Suh, Y.-E. Sung, Chem. Mater. 25 (2013) 1526–1532.
[11] M. Hara, J. Inukai, B. Bae, T. Hoshi, K. Miyatake, M. Uchida, H. Uchida, M. Watanabe, Electrochim. Acta 82 (2012) 277–283.
[12] A.K. Srouji, L.J. Zheng, R. Dross, A. Turhan, M.M. Mench, J. Power Sources 239 (2013) 433–442.
[13] L. Zheng, Q. Zeng, S. Liao, J. Zeng, Int. J. Hydrogen Energy 37 (2012) 13103–13109.
[14] Y.-I. Chou, Z.-Y. Siao, Y.-F. Chen, L.-Y. Sung, W.-M. Yang, C.-C. Wang, J. Power Sources 195 (2010) 536–540.
[15] G.-G. Park, Y.-J. Sohn, T.-H. Yang, Y.-G. Yoon, W.-Y. Lee, C.-S. Kim, J. Power Sources 131 (2004) 182–187.
[16] S.D. Knights, K.M. Colbow, J.-S. Pierre, D.-P. Wilkinson, J. Power Sources 127 (2004) 127–134.
[17] D. Liang, Q. Shen, M. Hou, Z. Shao, B. Yi, J. Power Sources 194 (2009) 847–853.
[18] D. Liang, M. Dou, M. Hou, Q. Shen, Z. Shao, B. Yi, J. Power Sources 196 (2011) 5595–5598.
[19] I.-C. Halalay, S. Swathirajan, B. Merzougui, M.-P. Balogh, G.-C. Garabedian, M.-K. Carpenter, J. Electrochem. Soc. 158 (2011) B313–B321.
[20] R.-H. Song, C.-S. Kim, D.-R. Shin, J. Power Sources 86 (2000) 289–293.
[21] A. Lundblad, P. Bjornbom, J. Electrochem. Soc. 139 (1992) 1337–1342.
[22] Z. Liu, L. Yang, Z. Mao, W. Zhuge, Y. Zhang, L. Wang, J. Power Sources 157 (2006) 166–176.
[23] J.-H. Ohs, U. Sauter, S. Maass, D. Stolten, J. Power Sources 196 (2011) 255–263.
[24] X.-G. Yang, Q. Ye, P. Cheng, Int. J. Hydrogen Energy 37 (2012) 14439–14453.
[25] T.-W. Patterson, R.M. Darling, Electrochem. Solid-State Lett. 9 (2006) A183–A185.
[26] W.R. Baumgartner, P. Parz, S.D. Fraser, J. Power Sources 182 (2008) 413–421.
[27] R.N. Carter, B.K. Brady, K. Subramanian, T. Tighe, H.A. Gasteiger, ECS Trans. 11 (2007) 423–433.
[28] P.T. Yu, W. Gu, R. Makharia, F.T. Wagner, H.A. Gasteiger, ECS Trans. 3 (2006) 797–809.
[29] W. Gu, R.N. Carter, P.T. Yu, H.A. Gasteiger, ECS Trans. 11 (2007) 963–973.
[30] T.R. Ralph, S. Hudson, D.P. Wilkinson, ECS Trans. 1 (2006) 67–84.
[31] Y.-H. Cho, T.-Y. Jeon, S.-J. Yoo, K.-S. Lee, M. Ahn, O.-H. Kim, Y.-H. Cho, J.-W. Lim, N. Jung, W.-S. Yoon, H. Choe, Y.-E. Sung, Electrochim. Acta 59 (2012) 264–269.
[32] A. Pozio, M.D. Francesco, A. Cemmi, F. Cardellini, L. Giorgi, J. Power Sources 105 (2002) 13–19.
[33] E.-A. Ticianelli, C.R. Derouin, S. Srinivasan, J. Electroanal. Chem. 251 (1998) 275–295.
[34] A. Taniguchi, T. Akita, K. Yasuda, Y. Miyazaki, J. Power Sources 130 (2004) 42–49.
[35] B. Avasarala, R. Moore, P. Haldar, Electrochim. Acta 55 (2010) 4765–4771.